Journal of Colloid and Interface Science 513 (2018) 53–61

Contents lists available at ScienceDirect

Journal of Colloid and Interface Science

journal homepage: www.elsevier.com/locate/jcis

Regular Article

Viscoelastic drops moving on hydrophilic and superhydrophobic surfaces

H. Xu [a], A. Clarke [b], J.P. Rothstein [c], R.J. Poole [a,*]

[a] School of Engineering, University of Liverpool, Liverpool L69 3GH, United Kingdom
[b] Schlumberger Gould Research, High Cross, Madingley Road, Cambridge CB3 0EL, United Kingdom
[c] Department of Mechanical and Industrial Engineering, University of Massachusetts Amherst, 160 Governors Drive, Amherst, MA 01003-2210, USA

GRAPHICAL ABSTRACT

ARTICLE INFO

Article history:
Received 26 July 2017
Revised 26 October 2017
Accepted 27 October 2017
Available online 28 October 2017

Keywords:
Superhydrophobic
Drops
Viscoelastic

ABSTRACT

So-called "superhydrophobic" surfaces are strongly non-wetting such that fluid droplets very easily roll off when the surface is tilted. Our interest here is in understanding if this is also true, all else held equal, for viscoelastic fluid drops. We study the movement of Newtonian and well-characterised constant-viscosity elastic liquids when various surfaces, including hydrophilic (smooth glass), weakly hydrophobic (embossed polycarbonate) and superhydrophobic surfaces (embossed PTFE), are impulsively tilted. Digital imaging is used to record the motion and extract drop velocity. Optical and SEM imaging is used to probe the surfaces. In comparison with "equivalent" Newtonian fluids (same viscosity, density surface tension and contact angles), profound differences for the elastic fluids are only observed on the superhydrophobic surfaces: the elastic drops slide at a significantly reduced rate and complex branch-like patterns are left on the surface by the drop's wake including, on various scales, beads-on-a-string-like phenomena. The strong viscoelastic effect is caused by stretching filaments of fluid from isolated islands, residing at pinning sites on the surface pillars, of order ~30 μm in size. On this scale, the local strain rates are sufficient to extend the polymer chains, locally increasing the extensional viscosity of the solution, retarding the drop.

* Corresponding author.
E-mail address: robpoole@liv.ac.uk (R.J. Poole).

https://doi.org/10.1016/j.jcis.2017.10.105
0021-9797/

1. Introduction

So-called "superhydrophobic" [1] surfaces have drawn a great deal of attention in recent decades because of their potential technical applications such as "self-cleaning" surfaces [2,3], friction-reduced surfaces for drag reduction (e.g., for hydrodynamically efficient ship design and "drag-reducing" pipe flows) and icephobic [4] surfaces for wind turbine blades. Such superhydrophobic surfaces have often taken inspiration from nature, such as from lotus and rice leaves [1]. Ollivier [5] first reported contact angles of nearly 180° on a surface coated with hydrophobic powders. Coghill and Anderson [6] found that stearic acid drops can achieve a contact angle as high as 160° on a rough surface of galena. This latter study showed the connection between wetting properties and surface roughness. Since those early studies, a number of conceptual models have been proposed to explain and help understanding of this connection between roughness and wetting, such as the well-known Wenzel [7] and Cassie–Baxter [8] models. From an understanding of this relationship, many studies have shown that superhydrophobicity can be produced by creating a micro or nano-scale structure on surfaces. In practice, superhydrophobic surfaces can be created by numerous means including physical methods [9–11], plasma methods [12–14], chemical methods [15–22], laser processes [23–25], photolithography [26–28] and polymer processes [29–35]. In this study, we create superhydrophobic surfaces by "hot-embossing" a fine wire mesh (wire diameter and spacing are approximately 30 μm) onto a hydrophobic polytetrafluoroethylene (PTFE) surface. The negative of the mesh structure is impressed on the PTFE surface to create superhydrophobicity with an advancing contact angle above 150° and low contact angle hysteresis. In such a manner, we can create relatively large surfaces (~0.15 by 0.15 m^2) in a quick, inexpensive and reproducible way. Throughout this paper we shall refer to such surfaces as the "xPTFE" surface.

One of the most famous and easily observed phenomenon of a superhydrophobic surface, the so-called "lotus effect" [3], is that small liquid drops can stand on such surfaces as an almost perfect spherical shape and move with apparently little to no effort. Although this phenomenon is simple to observe, it is difficult in practice to measure precisely when and how the drops begin to move. A range of studies have investigated the sliding [36–40] or rolling [39,41,42] of drops on various surfaces, but no study has investigated viscoelastic drops moving on superhydrophobic surfaces in detail so far. Note that, throughout this paper, we shall refer to the drops "moving" rather than attempt to categorise the motion as rolling or sliding [36–42]. Le Grand et al. [36] studied millimeter-sized Newtonian drops (silicone oil) on partially wetting surfaces with a static contact angle around 50°. The shape and motion of drops are characterized in four stages with increasing velocity or capillary number ($Ca = \eta U/\sigma$, where U is velocity, η is viscosity, σ is surface tension). At low velocity, the drops' contact line essentially maintains a round shape called the "oval" stage. With increasing velocity, the drop shape becomes more complex including a so-called "corner" transition stage and then onto "cusps" and then "pearling" at higher droplet velocities. Morita et al. [38] conducted a similar study but using two polymer solutions, a polystyrene of molecular weight M_w = 280,000 g/mol in acetophenone. A small difference observed with the comparator Newtonian fluid is that the polymer drop moves faster at equivalent capillary number, which may be due to the shear-thinning nature of the solutions but the use of the zero shear rate viscosity in the estimation of the capillary number. In addition to these studies which have directly examined the problem of moving viscoelastic drops on various surfaces, a number of previous studies have investigated the somewhat related problem of viscoelastic droplets impacting upon superhydrophobic surfaces [43–48].

In this paper, following a short letter which we recently published [49], we investigate moving viscoelastic drops on superhydrophobic and other surfaces in detail. In particular we examine a broader range of both surfaces and viscoelastic fluids, conduct additional analysis and use more refined imaging techniques than shown in our preliminary work [49]. In investigating droplet motion of viscoelastic fluids on superhydrophobic surfaces, an interesting phenomenon is observed. For water and other Newtonian fluid drops, the embossed structure on our superhydrophobic surfaces can reduce the friction by trapping air to form an air-liquid interface when a drop moves over, meanwhile the large contact angle of our surface leads to a small contact area between the fluid drops and the surface. In addition, the low contact angle hysteresis for these Newtonian drops on the xPTFE surface allow rapid movement when the surface is inclined (at angle α) above the rolling-off angle, as expected [8]. In this study, viscoelastic effects on moving drops are studied by using constant-viscosity viscoelastic liquids, so-called Boger fluids [50–52]. These have particular advantages for studying the effect of fluid elasticity independently of shear-thinning. By careful design, Boger fluids and a comparison Newtonian fluid can have essentially the same properties such as shear viscosity η, surface tension σ, density ρ, and advancing/receding contact angle $\theta_{adv}/\theta_{rec}$ on a given surface. When the drop moves on a hydrophilic surface, for example smooth glass, we find essentially no difference between the motion of these elastic liquids at identical capillary number and effective Bond number ($Bo = (V^{2/3}\rho g \cdot \sin\alpha)/\sigma$) where g is the gravitational acceleration. However, when a Boger fluid drop moves on our superhydrophobic surface, the velocity is significantly reduced in comparison with the Newtonian fluid at equivalent viscosity, and complex "branch-like" patterns, "beads-on-a-string" like phenomenon [53], are left on the surface. Such profound differences imply a complex mechanism during the motion of viscoelastic drops on superhydrophobic surfaces. In this paper we investigate this phenomenon in detail and on various scales (μm–mm).

The structure of the paper is as follows. Firstly, we describe the experimental set-up, including the manufacturing technique for our surfaces and the rheology of our working fluids. Subsequently, we describe extended results on the hydrophilic surface using a broader range of fluids and new results on a weakly hydrophobic surface followed by extended data for the xPTFE surfaces. In addition, we use enhanced SEM imaging to obtain greater insight into the surface structure and the underlying physical mechanism than was possible using standard light microscopy [49]. Finally, the paper ends with a short conclusions section.

2. Materials and methods

2.1. Manufacture of xPTFE surfaces

Many studies [9,10,12,18,25] have shown that superhydrophobicity can be produced by creating a rough structure on an initially-smooth polytetrafluoroethylene (PTFE) surface. In this study, a simple and inexpensive method is used to create superhydrophobicity on PTFE surfaces. Our approach is to use a very fine stainless steel mesh, the diameter of the mesh wire being tens of microns, as a model to emboss the PTFE sheet to create regular surface patterns. In this study, the embossing mesh has a wire diameter of 30 μm and wire density of 400 wires per inch. Prior to embossing, the PTFE sheet is cleaned with water, detergent and finally ethanol before being sanded using sandpaper to soften the surface sufficiently for the embossing process. Then the mesh is placed onto the PTFE sheet and sandwiched in between two 12

mm-thick stainless steel plates, 10 G-clamps were applied to hold the plates to provide uniform high pressure. Then the sample is heated in an oven at 350 °C, slightly higher than the quoted melting temperature of PTFE (328–346 °C [54]), for 3 h and allowed to cool down to room temperature for 8 h prior to removing the mesh which we found to be a useful measure in creating secondary roughness features. We observed no difference in the wetting properties of samples created in the oven with or without vacuum. The negative of the mesh is then embossed onto the PTFE surface, and Scanning Electron Microscopy (SEM) imaging is undertaken to show that the surfaces exhibit a pillar/brick-like structure which has an average size of 32 by 32 μm, the open area ratio (i.e. ratio of potential liquid-air interface to total area) is around 72% as shown by the SEM images for all surfaces used in Supplementary Materials Fig. S1. More complete information on how we obtained the SEM images are also given in the Supplementary Materials. Moreover, SEM also confirms that the embossing process does not significantly change the PTFE structure on top of the pillars/bricks when compared to the native PTFE sheet (compare Fig. S1 (b) and (d) for example). Superhydrophobic PTFE sheets with brick-like regular micro-structure and overall maximum size of 15 cm by 15 cm, limited by the dimension of the oven used, were created after this process. Static drops of Newtonian and Boger fluids have similar advancing/receding contact angles on the xPTFE surface being measured as about 150°/135° respectively using a fluid addition/removal method described in more detail in the Supplementary Materials, giving a contact angle hysteresis of about 15° for both fluids as shown in Table 1. The water drops can easily move-off the xPTFE surface due to the superhydrophobicity as expected as shown in supplementary movie #1. In order to isolate any potential effects of the surface structure, a weakly hydrophobic surface, a polycarbonate, was also embossed using the same mesh as used to emboss the xPTFE but at a lower temperature (~125 °C). The resulting surface has an advancing contact angle (~92°) and contact angle hysteresis (~38°) for both Newtonian and Boger fluids, which is not significantly different to the untreated polycarbonate surface, as is also shown in Table 1.

Video 1

2.2. Preparation of working fluids

Three Boger fluids, referred to as Fluids B1, B2 and B3, and a comparator Newtonian fluid, referred to as Fluid N1, were prepared in this study based on polyethylene glycol (PEG) (Table 2). Polyethylene glycol is a water-soluble polymer and has a large range of molecular weight from thousands to millions g/mol depending on different lengths of the molecular chain (above 20,000 g/mol it is termed polyethylene oxide "PEO"). The PEG solution exhibits practically no shear-thinning or elastic effects due to its low molecular weight, and produces a viscous Newtonian solution when dissolved in water. After adding a small amount of a high molecular-weight PEO polymer to a high concentration PEG solution, the water-PEG-PEO solution becomes a strongly-elastic Boger fluid [51]. More details on the fluids used can be found in the Supplementary Materials (Section S1.2).

2.3. Rheology of working fluids

Because the moving drop experiments were conducted at room temperature which varied slightly day to day (17–20 °C), the rheological profiles at different temperatures were measured in order to match exactly the experimental conditions. The shear viscosities of the four fluids were measured by an Anton Paar MCR 302 controlled-stress rheometer using a 60 mm diameter 1° cone-plate geometry at 17 °C and 20 °C, (shown in Fig. S2 in the Supplementary Materials). The relaxation time of the Boger fluids were measured using a Capillary Break Up Extensional Rheometer [55] (CaBER) at different temperatures. Details of the CaBER technique are provide in the Supplementary Materials (Section S1.2).

The working fluid characterisation includes viscosities, densities, surface tensions, and relaxation time of the four experimental fluids are listed in Table 2. As can be seen in Table 2, the four fluids have similar viscosities around 285 mPa·s at 20 °C when the shear rate is above about 5 s^{-1}. The CaBER measurements show the relaxation time λ of these Boger fluids have a large range from 0.2 s to 2.5 s and the extensional viscosity (not shown) also increases with the polymer molecular weight from 500 Pa·s for Fluid B1 to over 10,000 Pa·s for Fluid B3 (i.e., for Fluid B3 very similar to that measured in Oliveira and McKinley [53]). Fluids B2 and B3, which have the highest molecular weight, show a high elasticity and slight shear thinning especially at low shear rates. Meanwhile, the densities and surface tensions are very similar for all fluids due to the similar concentration of PEG and the same chemical components of the four solvents.

2.4. Inclined plate and drop motion recording system

An adjustable acrylic inclination platform was built to conduct the moving-drop experiments. The platform is fixed on a table and adjusted to the desired angle. Then the drops were placed on the test surface using a syringe pump to accurately control the drop volume. The flow rate of the syringe pump is carefully controlled at a very slow speed (10 μL/s) to prevent any potential

Table 1
Contact angles.

Surface	Boger fluid (fluid 3)			Newtonian fluid		
	Adv. contact angles θ_{Adv}	Rec. contact angles θ_{Rec}	Contact angle hysteresis	Adv. contact angles θ_{Adv}	Rec. contact angles θ_{Rec}	Contact angle hysteresis
Smooth glass	54°±5°	11°±5°	43°±10°	58°±5°	12°±5°	46°±10°
Smooth polycarbonate	90°±5°	55°±5°	35°±10°	88°±5°	55°±5°	32°±10°
Embossed polycarbonate	92°±5°	54°±5°	38°±10°	94°±5°	54°±5°	40°±10°
xPTFE	152°±5°	136°±5°	16°±10°	151°±5°	136°±5°	15°±10°

Table 2
Fluid properties.

Fluid	Shear viscosity η (mPa·s @20 °C)	Surface tension σ (mN/m)	Fluid density ρ (kg/m^3)	CaBER relaxation time λ (s)
Fluid B1: PEG/PEO (Boger $\lambda \sim 0.2$ s)	255 ± 2	53.3[a]	1080	0.2 ± 0.1
Fluid B2: PEG/PEO (Boger $\lambda \sim 1$ s)	285 ± 5	53.3[a]	1080	1 ± 0.5
Fluid B3: PEG/PEO (Boger $\lambda \sim 2.5$ s)	285 ± 5	53.3[a]	1080	2.5 ± 0.5
Fluid N1: PEG (Newtonian)	285 ± 2	53.3	1082	–

[a] Assumed same as solvent.

degradation of the polymer solutions via shear. The surface is then impulsively tilted and the droplet motion recorded using a camera (Nikon D5300) at 30 frames per second. The recording continues for at most 5 min, which avoids any significant influence of evaporation, and each experiment is repeated at least three times (a schematic of the setup is shown in Supplementary Materials as Fig. S4). In between each moving drop experiment the surface was gently cleaned with water and ethanol and then allowed to dry naturally. The recorded videos were post-processed using "Tracker" [57], to determine the steady-state droplet velocity. Hydrophilic smooth glass surfaces, microscope slides which were pre-cleaned and single use "as delivered", were used to directly compare with the hot-embossed superhydrophobic xPTFE surfaces. The advancing and receding contact angles for all of the test fluids on these glass surfaces are 54° and 11° respectively, as shown in Table 1. In addition, a weakly hydrophobic surface, a polycarbonate but embossed by the same mesh as used to emboss the xPTFE, was investigated as well to isolate any potential effect of the surface structure on the observed phenomena.

3. Results and discussion

3.1. Hydrophilic and weakly hydrophobic surfaces

Most surfaces in nature are hydrophilic [58], for example smooth glass surfaces, for such surfaces the contact angle is lower than 90°. Two Boger fluids, Fluids B2 and B3, and the Newtonian comparator, Fluid N1, with different controlled volumes of 50, 75 and 100 μL were tested on the smooth glass surface. The inclination angle of the surfaces was varied from 19° to 27°. In general, the Newtonian and Boger fluid drops behave very similarly on the smooth glass surfaces: they flow slowly, and leave a wide thin-film behind which indicates a close to zero receding contact angle. The velocity of the "drop" ranges from 0.05 mm/s for the lowest inclination angle and smallest volume to 0.8 mm/s for the highest inclination angle and largest volume. The data is plotted as velocity verses inclination angle in the Supplementary Materials as Fig. S5 where it can be seen that the velocity of the drops which have the same volume varies linearly with the inclination angle.

Although the viscosity of the Boger fluid is approximately constant with shear rate in most cases, a slight shear-thinning effect can be observed at very low shear rate (<5 s^{-1}). By adjusting the viscosity value based on a shear rate corresponding to the drop's moving speed and size (~0.01 s^{-1}), we can plot the data as capillary number versus Bond number, shown in Fig. 1, and all the data sets approximately collapse. This result is in agreement with previous studies [36,38], and this linear relationship between *Ca* and *Bo* with a non-zero intercept indicates a force balance between viscous force, gravitational and resistance caused by contact angle hysteresis. Even though the flow field inside the drop is complicated [39] while the drop is moving on the surface, under the relatively slow velocities observed here, the flow field may be considered as laminar and steady. For a deformed drop as it moves, viewed from above, it is possible to use either of the two primary axes to calculate an appropriate lengthscale (or an average of the two). However, for a drop leaving a film behind, as seen here, such calculations will likely be poor estimates. As a consequence, for simplicity we assume the drop is a hemisphere of radius *r*. Although we expect that the shear rate increases to infinity as the contact line is approached (because the height goes to zero), we try to capture that effect here by assuming that the drop's velocity will vary over some small distance δ which is proportional to this radius (expecting the constant of proportionality *c* to be << 1):

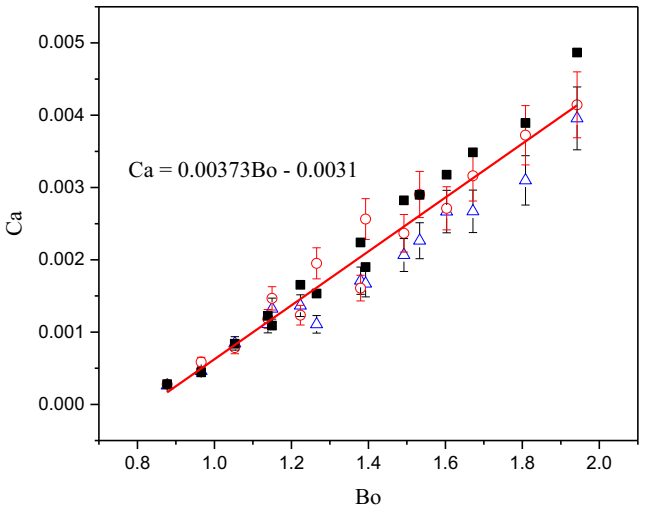

Fig. 1. Capillary number versus Bond number for Newtonian (■ Fluid N1) and Boger fluid (○ Fluid B2, $\lambda \sim 1$ s, and △ Fluid B3, $\lambda \sim 2.5$ s.) drops on smooth glass surface including linear fit to the complete data set. Error bars represent the spread of data from repeat experiments.

$$\dot{\gamma} \sim U/\delta \sim U/cr \tag{1}$$

And the contact area is then:

$$A \sim \pi r^2 \tag{2}$$

The viscous force can then be roughly estimated as

$$F_V \sim \eta \dot{\gamma} A = \frac{\eta U}{cr} \cdot \pi r^2 = \frac{\pi \eta U r}{c} \tag{3}$$

If we assume the volume of the drop is a hemisphere, the gravitational force is then:

$$F_g \sim \rho g V \sin\alpha = \rho g \frac{2}{3} \pi r^3 \sin\alpha \tag{4}$$

The resistance caused by contact angle hysteresis F_h is:

$$F_h \sim 2\sigma r(\cos\theta_{rec} - \cos\theta_{adv}). \tag{5}$$

If the viscous force balances with the gravitational force and contact angle hysteresis force, $F_g = F_v + F_h$, we have:

$$\rho g \frac{2}{3} \pi r^3 \sin\alpha \sim \frac{\eta U \pi r}{c} + 2\sigma r(\cos\theta_{rec} - \cos\theta_{adv}) \tag{6}$$

then if we divide both sides by $\pi\sigma r$, we have the relationship:

$$\frac{(\frac{2}{3}\pi)^{\frac{1}{3}}}{\pi} \frac{V^{2/3}\rho g \sin\alpha}{\sigma} \sim \frac{\eta U}{c\sigma} + \frac{2}{\pi}(\cos\theta_{rec} - \cos\theta_{adv}) \tag{7}$$

which is equivalent to $Ca \sim cC_1Bo - cC_2\,(\cos\theta_{rec} - \cos\theta_{adv})$, where C_1 is $\frac{(\frac{2}{3}\pi)^{\frac{1}{3}}}{\pi} \sim 0.41$ and C_2 is $\frac{2}{\pi} \sim 0.64$ (and $c << 1$). We note that, although the above analysis is rather simplified [59], the functional form of Eq. (7) is identical to others previously derived using more exact approaches [36–37]. This result demonstrates that under this experimental condition, the capillary number should be approximately proportional to the Bond number, and the slope is a constant for a particular surface somewhat analogous to a "friction coefficient", independent of the size or viscosity of the drop. The non-zero intercept of this linear curve is caused by the contact angle hysteresis. Based on this analysis the linear variation shown in Fig. 1 indicates the dominant forces achieved on the drop for these conditions are gravity, contact angle hysteresis and viscosity. Fitting the data shown in Fig. 1 can be used to estimate the value of the constant "c" and, as it can be determined separately from both the slope and the intercept, provide an indication of the internal consistency of the scaling analysis above. Doing so, assuming the receding contact angle is zero, gives values of c equal to 0.0092 and 0.010, calculated from the slope and intercept respectively. It should be noted that in the analysis above, and indeed throughout the paper, we do not try to account for the variation of the contact angle with the droplet velocity (i.e. by trying to define so-called "dynamic" contact angles). This is because previous studies of dynamic contact angle measurements of Newtonian fluids on superhydrophobic surfaces [48] showed that there was no variation of the advancing contact angle and only a very weak variation of the receding contact angle with contact line velocity or capillary number ($\theta_R \sim Ca^{1/9}$ instead of the expected dependency of $\theta_R \sim Ca^{1/3}$).

When a structure is created on a hydrophilic surface, the Wenzel state liquid-solid interface makes the surface more hydrophilic and could introduce some additional "friction" while drops move on the surface, acting like structural "roughness" elements [60,61]. To compare with the xPTFE surfaces which have a micro-scale brick-like surface structure, a polycarbonate plate was embossed by an identical mesh using a similar hot-embossing technique. The surface structure was observed using a microscope, and was found to be similar to the xPTFE structure (see Fig. S1 in Supplementary Materials). The velocity data for this embossed polycarbonate surface is shown in the Supplementary Materials as Fig. S6, and the velocities can be seen to be slower compared to the results on the smooth glass surface. The Boger fluid drops, much as was observed on the smooth glass surfaces, behave no differently to the Newtonian drops. In addition, all the data sets collapse in an approximately linear way when plotted as Ca versus Bo, as shown in Fig. 2. The intercept of the curve is close to the smooth glass data due to the similar level of contact angle hysteresis for the two surfaces (~38° for polycarbonate and ~43° for glass), but the slope is lower compared with the smooth glass results which is expected given the additional roughness introduced (c in this case is equal to 0.0057 and 0.0053, calculated from the slope and intercept respectively).

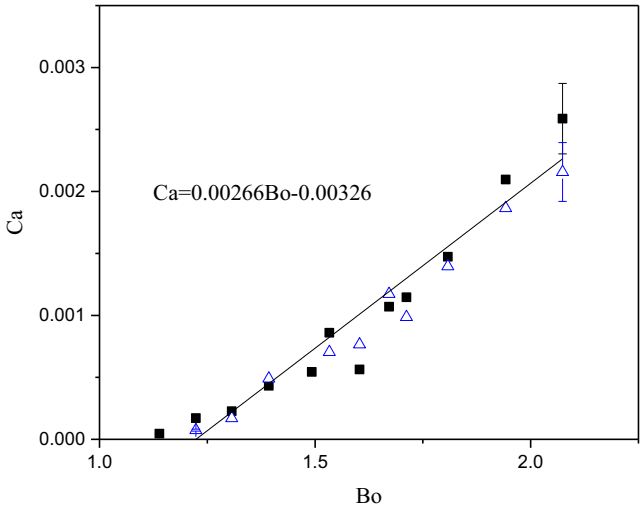

Fig. 2. Capillary number versus Bond number for Newtonian (■ Fluid N1) and Boger fluid (△ Fluid B3, $\lambda \sim 2.5$ s) drops on embossed polycarbonate surface including linear fit to the complete data set. Error bars represent the spread of data from repeat experiments.

3.2. Superhydrophobic surfaces

In contrast to hydrophilic surfaces, the contact angles on superhydrophobic surfaces are much higher than 90°, therefore the surface tension acts to reduce the contact interface area. In addition, the contact angle hysteresis is quite small (<15°) and, as a consequence, the drops can move much more easily than on hydrophilic and weakly hydrophobic surfaces such as those discussed in Section 3.1. This is especially so on superhydrophobic surfaces which have typical contact angles higher than 145° [1], the speed of movement is often over 10 times greater than that on hydrophilic surfaces. On the superhydrophobic xPTFE surfaces, the velocities of our Newtonian drops were slower than the maximum wetting speed [36,62] hence no instability is observed and no threads are left behind for these drops. In contrast, the Boger fluid drops are slowed down significantly compared to the Newtonian drops and there are complex "branch-like" and "beads-on-tail" structures left behind, as shown in Fig. 3 and supplementary movie #2, which indicates a distinctive mechanism for such elastic fluids on superhydrophobic surfaces in comparison to equivalent Newtonian fluids.

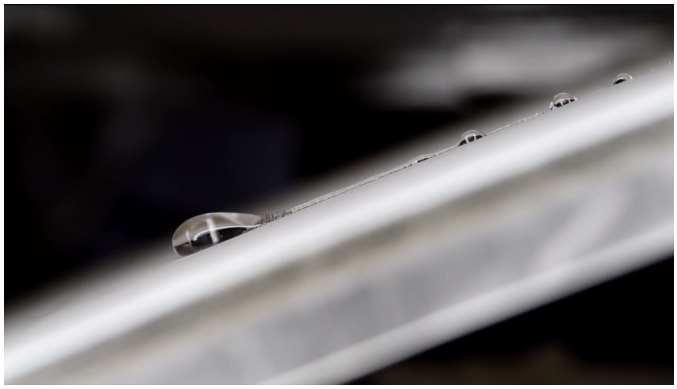

Video 2

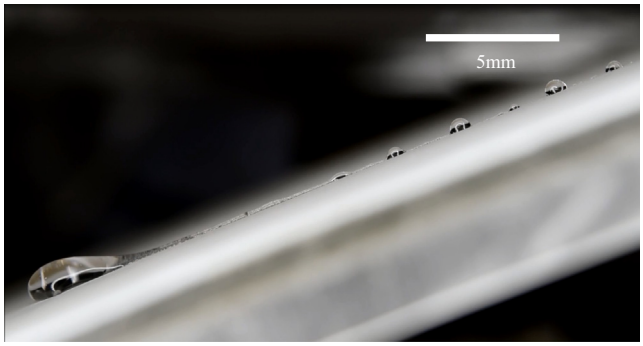

Fig. 3. Image highlighting view of "Beads-on-tail" structure left behind moving Boger fluid drop. Drop movement direction was from top right to bottom left. For movie of drop motion see supplementary movie #2.

Two Boger fluids, Fluids B1 and B3, and a Newtonian comparator Fluid N1 were tested on the xPTFE surfaces. The volumes of the drop were controlled via a syringe pump as 50, 75 and 100 μL and the inclination angle of the surfaces is varied from 19° to 27°. The velocity versus inclination angle data is shown in the Supplementary Materials as Fig. S7. The velocity of the Newtonian drops is much higher than that of equivalent volume drops on hydrophilic surfaces, the range is from 2 mm/s, at lowest inclination angle and smallest volume, to 15 mm/s at the highest inclination angle and largest volume. For the Boger fluid drops, the velocity is much lower than the Newtonian drops, being reduced by nearly 50% for the low elasticity fluid (Fluid B1) and 85% for the highly-elastic fluid (Fluid B3). If plotted as *Ca* versus *Bo*, shown in Fig. 4, the data sets collapse for each type of fluid respectively, but the data from different fluids do not collapse onto a single master curve as was observed for the smooth and rough hydrophilic surfaces. Assuming identical viscous forces, the three slopes indicate three different "friction coefficients" on the same surface, and the only difference between these fluids is the level of elasticity. We note here that our Newtonian drops are initially larger than the capillary length and therefore this linear scaling is expected [41]. Comparing the data of Fluid B1 and B3 which have different elasticity, the larger elasticity exhibits a larger "friction coefficient", which means the elasticity essentially increases the "friction" and slows the drops down more. After calculating the apparent viscosity, shown in Supplementary Materials as Fig. S8, by comparing the sliding velocity of Boger fluid drops to the Newtonian drops (assuming the resistance is caused solely by higher apparent "viscosity"), for the lower molecular weight Boger fluid (Fluid B1) its apparent viscosity is almost 2.5 times the Newtonian one, for the higher molecular weight Boger fluid (fluid B3) its apparent viscosity is as high as 7 times the Newtonian drop at low speeds and decreasing to 2.5 times when the Bond number is over 1.4. Meanwhile, if we estimate a Weissenberg number ($Wi = \dot{\gamma} \cdot \lambda$) to examine the effect of elasticity, we note that the speed of smaller Boger drops on the xPTFE surface is roughly similar to large drops on smooth glass surface. This suggests that they have the same range of "global" Weissenberg number *Wi* (~0.8), which based on drop speed and drop radius (~2–4 mm) or capillary length (~2.2 mm) in these experiments, but as we have demonstrated in Section 3.1, there is no effect of elasticity observed on either smooth glass or embossed polycarbonate surfaces. This suggests elastic effects, which were only observed on the xPTFE surfaces, cannot be explained as a "bulk" effect even though the Weissenberg number is order one on both smooth glass, embossed polycarbonate and superhydrophobic surfaces. Considering the micro-scale structure of the xPTFE surface and the "branch-like" tail of the Boger fluid left by the moving drop, we suspect that the strong elastic effect might possibly be caused by a micro-scale mechanism i.e. interaction between the fluid and the surface on the scale of the brick-like structure (~30 μm). In order to gain more insight into this phenomenon, we used both light microscope (Nikon Epiphot TME) and SEM to investigate the "branch-like" structures on the drop's "tail", as is shown in Fig. 5.

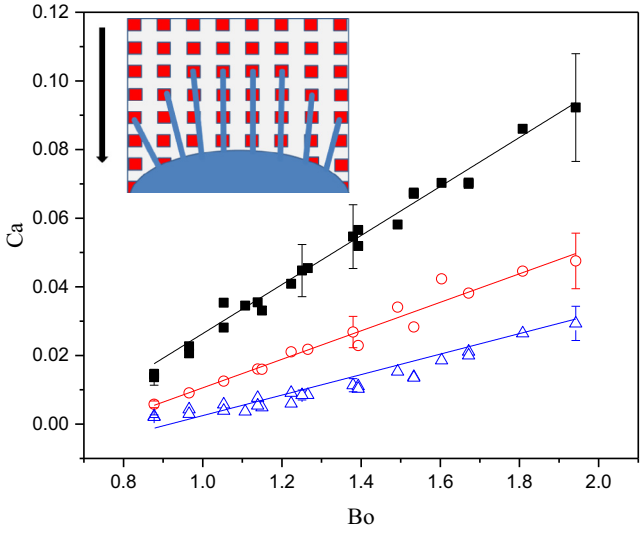

Fig. 4. Capillary number versus Bond number for Newtonian (■ fluid N1) and Boger fluid (○ Fluid B1, λ ~ 0.2 s, and △ Fluid B3, λ ~ 2.5 s) drops on xPTFE including representative error bars and linear fits to each of the data sets. Error bars represent the spread of data from repeat experiments. Inset shows cartoon of possible polymer extension mechanism on xPTFE.

3.3. Micro-scale filaments extension

Using microscopy to investigate the "branch-like" structure which is left behind the drop, under the optical microscope, it is shown that filaments connect the isolated micro-scale size droplets pinned to the pillars that form the surface structure (size on the order of 30 μm), as can be seen in Fig. 5(a). Using SEM, which benefits from higher resolution and better depth of field, the surface structure and droplets were more clearly observed. However, the solvent evaporates due to the fact that the samples have to be placed in a vacuum chamber during the SEM investigation. Although only dried polymer was observed, the drops and the filaments connecting between them are still clearly observable as shown in Fig. 5(b)–(d). This suggests that during the drop's movement on the xPTFE surface, while the drop is passing over the pillar, some of the fluid is "pinned" on the sharp corner of the pillar to form a separate droplet still connected to the main drop via a filament. We posit that, within this stretching filament, the local strain rate is sufficient to extend the polymer chains between the micro scale drop and the main drop. The extending chains increase the extensional viscosity locally in this filament, slowing down the drop and leaving behind the "branch-like" structure when the filaments finally breaks due to capillarity. Kumpfer and McCarthy [56] studied a comparable mechanism on similar superhydrophobic surfaces, but only for water. Their study shows the microdroplets can be produced at pining sites on this kind of surface and then rapidly evaporate corroborating this picture. The extension of the filaments provides a tensile resistive force to the main drop and that is the reason why the Boger fluid drops are significantly slowed down compared to the Newtonian drops, very much akin to a series of "bungy" ropes pulling against the main drop. For this to be true, the filament break-up time $\tau_b \approx \eta_E d/\sigma$ must be longer than the time for the drop to reach to the next pillar, $\tau_c = w/U$. Here $w = 2d$ is the spacing between pillars. Therefore, a minimum extensional viscosity of $\eta_E > 2\sigma/U \approx 100$ Pa·s is required for this to form stable filaments between the pillar and main drop, from the CaBER measurements the extensional viscosities (500 Pa·s and 10,000 Pa·s) of the two Boger fluid used in this study are much larger than this requirement. To estimate the resistance force from the extension of these filaments, as shown as a cartoon in the inset in Fig. 4, the resistance force resulting from extensional viscosity can be approximated as $F_{EV} = \eta_E \dot{\varepsilon} k A$, where $\dot{\varepsilon} = U/w$ is the extension rate, k is the probability of Boger fluid attaching on the pillars of the surface structure, and $A = \pi d^2 n/4$ is the total area of the pillars through the receding contact line of the drop, where $n=D/2w$ is the number of pillars along that line. Then the force becomes $F_{EV} = (\pi U k D \eta_E)/16 = (\pi k \sigma D/16) Tr Ca$ where $Tr = \eta_E/\eta$ is the Trouton ratio. As the geometry of the surface features appears to cancel out from this expression, we expect the probability for fluid to remain attached (k) will not be a constant but be dependent on

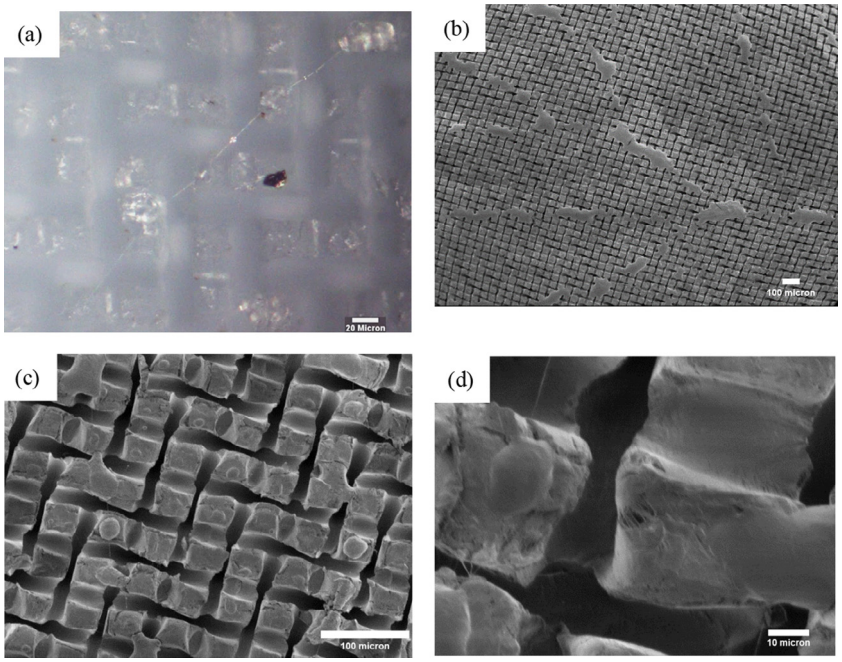

Fig. 5. (a) Branch-like structure left on the xPTFE surface observed under optical microscope (200× magnification) illustrating islands of elastic fluid marooned on pillars of structure connected by very thin (~1 μm) fluid bridges. (b) 45× magnification; (c) 250× magnification; (d) 1200× magnification, observed under SEM, polymer "blobs" attached to the pillars and filaments connected between them.

the precise size and layout of the embossed features. From microscope images, it can be seen that k is on the order of 0.1 for this surface and the resulting extensional force from the extension of the filaments is then on the same order of magnitude as the gravitational force and shear viscosity force. The extension process of these filaments causes some of the fluid to be slowed down, and form an elongated tail. The resulting "beads-on-a-tail" phenomenon then occurs possibly by a similar instability mechanism as observed in capillary break-up experiments [63] and ink-jetting processes [64,65]. Experiments on the weakly hydrophobic (polycarbonate) surface with a similar micro-scale structure, discussed in Section 3.1, do not exhibit these phenomena. In addition, similar experiments were conducted on another superhydrophobic surface. This surface is manufactured by using an ethanolic suspension of perfluorosilane-coated titanium dioxide particles and has a random surface texture [22]. Similar phenomena, i.e. slowed down Boger fluid drops and "beads-on-tail" residue, were observed on these superhydrophobic surfaces also indicating the robustness of our observations for different superhydrophobic surfaces. In totality, these combined results indicate that roughness alone is insufficient to create this mechanism but that the combination of hydrophobicity with surface topology (the hallmark of superhydrophobic surfaces), are *both* required to observe such striking phenomena.

4. Conclusions

Under our experimental conditions, Boger fluid drops with very high elasticity but otherwise identical properties show no difference compared to Newtonian fluid drops while moving on hydrophilic glass surfaces. The main force balance in such cases is between viscosity, gravity and contact angle hysteresis. In addition, embossing structure on a weakly hydrophobic polycarbonate surface only increases the "friction", retarding the speed of the drops, but is otherwise unremarkable. These results are in approximate agreement with the limited previous results of droplet motion of non-Newtonian fluids [38,40] on such surfaces.

On the basis on many previously reported studies on the wetting properties of so-called superhydrophobic surfaces [1–3] it would be anticipated that fluid droplets placed on the surface would rapidly roll-off the surface when impulsively tilted above some critical angle [41,42]. This work has highlighted that, although this is true even for quite viscous Newtonian droplets (~280 mPa·s or 280 times more viscous than water), it is certainly *not true* for highly-elastic viscoelastic fluids even when the shear viscosity, density and surface tension is matched to the Newtonian fluid drop. On superhydrophobic surfaces (hot-embossed xPTFE), the elastic drops move at a significantly reduced rate (up to ~85% reduction). "Branch-like" structures were left behind the drop and a "beads-on-tail" instability forms on that tail. Thus significant fluid residue is left on surfaces which are nominally "non-wetting". Even though a "global" Weissenberg number, based on drop speed and droplet radius or the capillary length, is order one this cannot fully explain such pronounced viscoelastic effects as at similar Weissenberg numbers on other surfaces no differences were seen. Using optical microscopy and SEM, a phenomenon was observed which indicates the local extension of single filaments between the main drop and micro drops pinned on individual surface pillars producing significant resistance to the drop's motion. This phenomenon requires the combination of both surface topology and hydrophobicity (i.e. the surface to be superhydrophobic). In addition, the higher elasticity provides a larger resistance force from this effect.

Our results presented here, in combination with our limited preliminary results [49], are the first to indicate that "super hydrophobic" surfaces may lose some of their beneficial properties when interacting with elastic fluids. The limited previous studies of droplet motion of non-Newtonian fluids [38,40], admittedly only on smooth hydrophobic and weakly hydrophobic surfaces, would not have suggested any such extravagant effects with non-Newtonian fluids with these cases indicating only subtle differences. Our results indicate that, even if for such viscoelastic fluids they exhibit high contact angles and low contact angle hysteresis, such surfaces may not be "non-wetting" for viscoelastic fluids as significant fluid

residue is left behind. Given the large interest in such superhydrophobic surfaces e.g. [66–69], and their many potential practical applications, our results should be of wide interest as these surfaces may not respond as expected when interacting with viscoelastic fluids. This is especially important for any potential applications as many fluids used in practical coating flows are viscoelastic (e.g. paints, inks), as are many biological liquids.

Future work in this area should investigate a broader range of superhydrophobic surfaces and viscoelastic fluids (including, for example, shear-thinning effects) to determine the ubiquity of the phenomena observed here. We have made a tentative effort in this direction, using superhydrophobic surfaces made from TiO_2 [22], and these surfaces were also observed to exhibit similar effects. Finally, it may be possible to utilise this striking phenomena to *quantify* viscoelastic effects by relating speed reduction on the surface at a given angle to, say, the fluid's extensional viscosity.

Acknowledgments

We would like to thank Dr. Colin Crick (University of Liverpool) for producing the random surface texture superhydrophobic surface [22] referred to in section 3.3. We would also like to thank Dr. Karl Dawson (University of Liverpool) for his help obtaining the SEM images. RJP would like to thank the Engineering and Physical Sciences Research Council (EPSRC) for the award of a Fellowship under grant EP/M025187/1.

Appendix A. Supplementary data

Supplementary data associated with this article can be found, in the online version, at https://doi.org/10.1016/j.jcis.2017.10.105.

References

[1] N.J. Shirtcliffe, G. McHale, S. Atherton, M.I. Newton, An introduction to superhydrophobicity, Adv. Colloid Interface Sci. 161 (2010) 124–138.
[2] Y.T. Cheng, D.E. Rodak, Is the lotus leaf superhydrophobic?, Appl Phys. Lett. 86 (2005) 1–3.
[3] C. Neinhuis, W. Barthlott, Characterization and distribution of water-repellent, self-cleaning plant surfaces, Ann. Bot. 79 (1997) 667–677.
[4] M. Nosonovsky, V. Hejazi, Why superhydrophobic surfaces are not always icephobic, ACS Nano. 6 (2012) 8488–8491.
[5] H. Ollivier, Recherches sur la capillarité, J. Phys. Théorique Appliquée 6 (1907) 757–782.
[6] W.H. Coghill, C.O. Anderson, US, Bur, Mines, Tech. Pap. 47, 1923, 262.
[7] R.N. Wenzel, Resistance of solid surfaces to wetting by water, J. Ind. Eng. Chem. 28 (1936) 988–994.
[8] A.B.D. Cassie, S. Baxter, Wettability of porous surfaces, Trans. Faraday Soc. 40 (1944) 546–551.
[9] J. Zhang, J. Li, Y. Han, Superhydrophobic PTFE surfaces by extension, Macromol. Rapid Commun. 25 (2004) 1105–1108.
[10] M.A. Nilsson, R.J. Daniello, J.P. Rothstein, A novel and inexpensive technique for creating superhydrophobic surfaces using Teflon and sandpaper, J. Phys. D. Appl. Phys. 43 (2010) 45301.
[11] G.D. Bixler, B. Bhushan, Bioinspired micro/nanostructured surfaces for oil drag reduction in closed channel flow, Soft Matter. 9 (2013) 1620.
[12] M. Morra, E. Occhiello, F. Garbassi, Contact angle hysteresis in oxygen plasma treated poly(tetrafluoroethylene), Langmuir 5 (1989) 872–876.
[13] J.-Y. Shiu, C.-W. Kuo, P. Chen, Fabrication of tunable superhydrophobic surfaces, Chem. Mater. 5648 (2004) 325–332.
[14] S.H. Kim, J.-H. Kim, B.-K. Kang, H.S. Uhm, Superhydrophobic CFx coating via in-line atmospheric RF plasma of He-CF4-H2, Langmuir 21 (2005) 12213–12217.
[15] L. Jiang, Y. Zhao, J. Zhai, A lotus-leaf-like superhydrophobic surface: a porous microsphere/nanofiber composite film prepared by electrohydrodynamics, Angew. Chem. Int. Ed. Engl. 43 (2004) 4338–4341.
[16] K. Acatay, E. Simsek, C. Ow-Yang, Y.Z. Menceloglu, Tunable, superhydrophobically stable polymeric surfaces by electrospinning, Angew. Chem. Int. Ed. Engl. 43 (2004) 5210–5213.
[17] N.J. Shirtcliffe, G. McHale, M.I. Newton, G. Chabrol, C.C. Perry, Dual-scale roughness produces unusually water-repellent surfaces, Adv. Mater. 16 (2004) 1929–1932.
[18] Y. Kunugi, T. Nonaku, Y.B. Chong, N. Watanabe, Electro-organic reactions on organic electrodes. Part 18. Electrolysis using composite-plated electrodes. Part VII. Preparation of ultrahydrophobic electrodes and their electrochemical properties, J. Electroanal. Chem. 353 (1993) 209–215.
[19] J.T. Han, Y. Jang, D.Y. Lee, J.H. Park, S.-H. Song, D.-Y. Ban, K. Cho, Fabrication of a bionic superhydrophobic metal surface by sulfur-induced morphological development, J. Mater. Chem. 15 (2005) 3089.
[20] E. Hosono, S. Fujihara, I. Honma, H. Zhou, Superhydrophobic perpendicular nanopin film by the bottom-up process, J. Am. Chem. Soc. 127 (2005) 13458–13459.
[21] B. Qian, Z. Shen, Fabrication of superhydrophobic surfaces by dislocation-selective chemical etching on aluminum, copper, and zinc substrates, Langmuir 21 (2005) 9007–9009.
[22] Y. Lu, S. Sathasivam, J. Song, C.R. Crick, C.J. Carmalt, I.P. Parkin, Robust self-cleaning surfaces that function when exposed to either air or oil, Science 347 (2015) 1132–1135.
[23] M.T. Khorasani, H. Mirzadeh, Z. Kermani, Wettability of porous polydimethylsiloxane surface: morphology study, Appl. Surf. Sci. 242 (2005) 339–345.
[24] X. Song, J. Zhai, Y. Wang, L. Jiang, Fabrication of superhydrophobic surfaces by self-assembly and their water-adhesion properties, J. Phys. Chem. B. 109 (2005) 4048–4052.
[25] S. Falah Toosi, S. Moradi, S. Kamal, S.G. Hatzikiriakos, Superhydrophobic laser ablated PTFE substrates, Appl. Surf. Sci. 349 (2015) 715–723.
[26] J. Ou, B. Perot, J.P. Rothstein, Laminar drag reduction in microchannels using ultrahydrophobic surfaces, Phys. Fluids. 16 (2004) 4635.
[27] C.-H. Choi, U. Ulmanella, J. Kim, C.-M. Ho, C.-J. Kim, Effective slip and friction reduction in nanograted superhydrophobic microchannels, Phys. Fluids. 18 (2006) 87105.
[28] Z.-Z. Gu, H. Uetsuka, K. Takahashi, R. Nakajima, H. Onishi, A. Fujishima, O. Sato, Structural color and the lotus effect, Angew. Chem. Int. Ed. Engl. 34 (2003) 891–894.
[29] K.K.S. Lau, J. Bico, K.B.K. Teo, M. Chhowalla, G.A.J. Amaratunga, W.I. Milne, G.H. McKinley, K.K. Gleason, Superhydrophobic carbon nanotube forests, Nano Lett. 3 (2003) 1701–1705.
[30] P. Joseph, C. Cottin-Bizonne, J.-M. Benoît, C. Ybert, C. Journet, P. Tabeling, L. Bocquet, Slippage of water past superhydrophobic carbon nanotube forests in microchannels, Phys. Rev. Lett. 97 (2006) 156104.
[31] N.J. Shirtcliffe, G. McHale, M.I. Newton, C.C. Perry, Intrinsically superhydrophobic organosilica sol-gel foams, Langmuir 19 (2003) 5626–5631.
[32] H.Y. Erbil, A.L. Demirel, Y. Avci, O. Mert, Transformation of a simple plastic into a superhydrophobic surface, Science 299 (2003) 1377–1380.
[33] J.T. Han, Y. Zheng, J.H. Cho, X. Xu, K. Cho, Stable superhydrophobic organic-inorganic hybrid films by electrostatic self-assembly, J. Phys. Chem. B. 109 (2005) 20773–20778.
[34] H. Yabu, M. Shimomura, Single-step fabrication of transparent superhydrophobic porous polymer films, Chem. Mater. 11 (2005) 5231–5234.
[35] L. Gao, T.J. McCarthy, A perfectly hydrophobic surface (θ A/θ R = 180°/180°), J. Am. Chem. Soc. 128 (2006) 9052–9053.
[36] N. Le Grand, A. Daerr, L. Limat, Shape and motion of drops sliding down an inclined plane, J. Fluid Mech. 541 (2005) 293.
[37] H.-Y. Kim, H.J. Lee, B.H. Kang, Sliding of liquid drops down an inclined solid surface, J. Colloid Interface Sci. 247 (2002) 372–380.
[38] H. Morita, S. Plog, T. Kajiya, M. Doi, Slippage of a droplet of polymer solution on a glass substrate, J. Phys. Soc. Japan 78 (2009) 1–4.
[39] S.R. Hodges, O.E. Jensen, J.M. Rallison, Sliding, slipping and rolling: the sedimentation of a viscous drop down a gently inclined plane, J. Fluid Mech. 512 (2004) 95–131.
[40] S. Varagnolo, G. Mistura, M. Pierno, M. Sbragaglia, Sliding droplets of Xanthan solutions: a joint experimental and numerical study, (n.d.) 1–8.
[41] D. Richard, D. Quéré, Viscous drops rolling on a tilted non-wettable solid, Europhys. Lett. 48 (1999) 286–291.
[42] B.M. Mognetti, H. Kusumaatmaja, J.M. Yeomans, Drop dynamics on hydrophobic and superhydrophobic surfaces, (n.d.) 1–20.
[43] V. Bergeron, D. Bonn, J.Y. Martin, L. Vovelle, Controlling droplet deposition with polymer additives, Nature 405 (2000) 772–775.
[44] Y. Son, C. Kim, Spreading of inkjet droplet of non-Newtonian fluid on solid surface with controlled contact angle at low Weber and Reynolds numbers, J. Non-Newtonian Fluid Mech. 162 (2009) 78–87.
[45] V. Bertola, Dynamic wetting of dilute polymer solutions: the case of impacting droplets, Adv. Colloid Interface Sci. 193 (2013) 1–11.
[46] M.I. Smith, J.S. Sharp, Origin of contact line forces during the retraction of dilute polymer solution drops, Langmuir 30 (2014) 5455–5459.
[47] D. Izbassarov, M. Muradoglu, Effects of viscoelasticity on drop impact and spreading on a solid surface, Phys. Rev. Fluids 1 (2016) 023302.
[48] J.H. Kim, H.P. Kavehpour, J.P. Rothstein, Dynamic contact angle measurements on superhydrophobic surfaces, Phys. Fluids 27 (2015) 032107.
[49] H. Xu, A. Clarke, J.P. Rothstein, R.J. Poole, Sliding viscoelastic drops on slippery surfaces, Appl. Phys. Lett. 108 (2016) 241602.
[50] D.V. Boger, A highly elastic constant-viscosity fluid, J. Non-Newton Fluid Mech. 3 (1977) 87–91.
[51] P. Dontula, C.W. Macosko, L.E. Scriven, Model elastic liquids with water-soluble polymers, AIChE J. 44 (1998) 1247–1255.
[52] D.F. James, Boger Fluids, Annu. Rev. Fluid Mech. 41 (2009) 129–142.
[53] M.S.N. Oliveira, G.H. McKinley, Iterated stretching and multiple beads-on-a-string phenomena in dilute solutions of highly extensible flexible polymers, Phys. Fluids 17 (2005) 1–4.

[54] H.W. Starkweather, P. Zoller, G.A. Jones, The heat of fusion of poly(ethylene terephthalate), J. Polym. Sci. Polym. Phys. Ed. 21 (1983) 295–299.
[55] L.E. Rodd, T.P. Scott, J.J. Cooper-White, G.H. McKinley, Capillary break-up rheometry of low-viscosity elastic fluids, Appl. Rheol. 15 (2005) 12–27.
[56] J.W. Krumpfer, T.J. McCarthy, Dip-coating crystallization on a superhydrophobic surface: a million mounted crystals in a 1 cm^2 array, J. Am. Chem. Soc. 133 (2011) 5764–5766.
[57] D. Brown, A.J. Cox, Innovative uses of video analysis, Phys. Teach. 47 (2009) 145.
[58] J. Drelich, E. Chibowski, D.D. Meng, K. Terpilowski, Hydrophilic and superhydrophilic surfaces and materials, Soft Matter 7 (2011) 9804.
[59] J.H. Snoeijer, B. Andreotti, Moving contact lines: scales, regimes, and dynamical transitions, Ann. Rev. Fluid Mech. 45 (2013) 269–292.
[60] G. Whyman, E. Bormashenko, T. Stein, The rigorous derivation of Young, Cassie-Baxter and Wenzel equations and the analysis of the contact angle hysteresis phenomenon, Chem. Phys. Lett. 450 (2008) 355–359.
[61] C. Lee, C.H. Choi, C.J. Kim, Superhydrophobic drag reduction in laminar flows: a critical review, Exp. Fluids. 57 (2016) 1–20.
[62] T.D. Blake, K.J. Ruschak, A maximum speed of wetting, Nature 282 (1979) 489–491.
[63] M.S.N. Oliveira, R. Yeh, G.H. McKinley, Iterated stretching, extensional rheology and formation of beads-on-a-string structures in polymer solutions, J. Non-Newton Fluid Mech. 137 (2006) 137–148.
[64] The stability of ink-jet printed lines of liquid with zero receding contact angle on a homogeneous substrate, 477 (2003) 175–200.
[65] S.H. Davis, Moving contact lines and rivulet instabilities. Part 1. The static rivulet, J. Fluid Mech. 98 (1980) 225–242.
[66] X. Zhao, B. Yu, J. Zhang, Transparent and durable superhydrophobic coatings for anti-bioadhesion, J. Colloid Interface Sci. 501 (2017) 222–230.
[67] Q. Wen, F. Guo, F. Yang, Z. Guo, Green fabrication of coloured superhydrophobic paper from native cotton cellulose, J. Colloid Interface Sci. 497 (2017) 284–289.
[68] S. Leclear, J. Leclear, K. Park, W. Choi, Drop impact on inclined superhydrophobic surfaces, J. Colloid Interface Sci. 461 (2016) 114–121.
[69] M.S. Khalil-abad, M.E. Yazdanshenas, Superhydrophobic antibacterial cotton textiles, J. Colloid Interface Sci. 351 (2010) 293–298.